Particuology 115 (2026) 256–266

Contents lists available at ScienceDirect

Particuology

journal homepage: www.elsevier.com/locate/partic

Isothermal sorption-enhanced biomass gasification for hydrogen-rich syngas production using $SrMnO_3$ redox-activated CO_2 sorbents in a fluidized bed

Runxia Cai[a,1,2], Mahe Rukh[a,1], Andrew Jones[b], Leo Brody[a], Alexandra Pierce[a], Mahdi Niknam Shahrak[a], Stephen Kelly[b], Sunkyu Park[b,*], Fanxing Li[a,**]

[a] Department of Chemical and Biomolecular Engineering, North Carolina State University, Raleigh, NC 27695-7905, USA
[b] Department of Forest Biomaterials, North Carolina State University, Raleigh, NC 27695-7905, USA

HIGHLIGHTS

- Redox-active sorbent enables isothermal sorption enhanced steam gasification (SESG).
- Isothermal SESG leads to six-fold increase in H_2 yield.
- $SrMnO_{3-\delta}$ shows excellent cyclic stability and ash tolerance.
- SESG improves cold gas efficiency with better syngas quality.

GRAPHICAL ABSTRACT

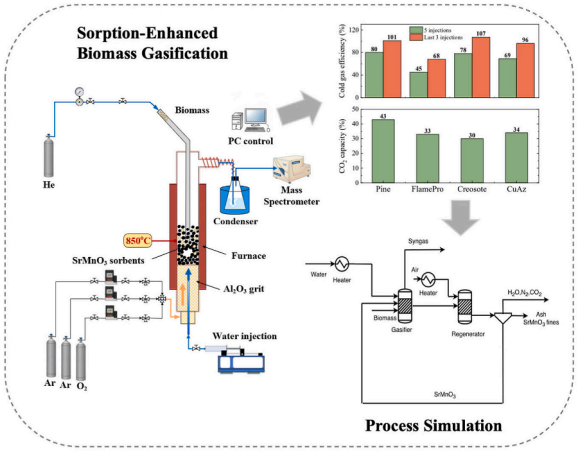

ARTICLE INFO

Keywords:
Gasification
Hydrogen
Sorbent
Carbon dioxide
Fluidized bed

ABSTRACT

Sorption-enhanced steam gasification (SESG) represents a promising route for hydrogen-rich syngas production. However, the rapid deactivation of conventional CaO-based sorbents, and the efficiency loss associated with the high temperature sorbent regeneration step, remain as critical challenges. In this study, a redox-activated $SrMnO_3$ sorbent was used for isothermal SESG of biomass in a fluidized-bed to investigate fuel flexibility, torrefaction effects, and long-term stability. Four biomass feedstocks as well as their torrefied counterparts were evaluated. All untreated feedstocks produced hydrogen-rich syngas with H_2 concentration >60% and H_2/CO

This article is part of a special issue entitled: SI honoring Profs. Jin & Yu published in Particuology.

* Corresponding author.
** Corresponding author.
E-mail addresses: spark@ncsu.edu (S. Park), fli5@ncsu.edu (F. Li).
[1] These authors contributed equally to this work.
[2] Present address: School of Mechanical Engineering, Shanghai Jiao Tong University, Shanghai 200240, China.

https://doi.org/10.1016/j.partic.2026.05.018
Received 8 April 2026; Received in revised form 22 May 2026; Accepted 24 May 2026
Available online 29 May 2026

ratios >4 under isothermal operation at 850 °C. Torrefaction decreased H_2 purity and syngas yield due to reduced volatile matter content. Long-term experiments in both a fluidized-bed reactor and TGA demonstrated excellent cyclic stability of $SrMnO_3$ and strong ash resistance. The structural and compositional properties of the sorbents were characterized in detail, confirming the chemical and structural stability of the $SrMnO_3$ sorbent during prolonged cyclic operation. Process simulation further showed that SESG of biomass significantly enhanced cold gas efficiency while maintaining a comparable heat demand compared to state-of-the-art indirect biomass gasification. Overall, $SrMnO_3$ exhibits strong potential as a robust sorbent for efficient and flexible biomass-to-hydrogen conversion.

1. Introduction

With the increasing impacts of global warming, reducing greenhouse gas emission has emerged as a prominent global concern (Mac Dowell et al., 2021). Due to the merits in the high specific energy density and environmentally friendly byproducts, hydrogen is being widely regarded as a highly promising substitute for conventional energy carriers (Acar & Dincer, 2020; da Silva Veras et al., 2017; Yue et al., 2021). It is widely used as an intermediate for chemical synthesis and also served as an energy carrier for heat and power generation (Antzaras & Lemonidou, 2022; Hanley et al., 2018; Hosseini & Wahid, 2016). In 2024, the global hydrogen supply reached ~100 million tons, with a projection to be 130~180 million tons by 2030 (Gül et al., 2025). However, the low-CO_2-emssion hydrogen only accounted for <1% of the total global production, with a majority still produced from fossil fuels (Zapantis, 2021). As such, the conventional production pathway remains carbon-intensive despite the clean features of hydrogen (Dawood et al., 2020; Sazali, 2020).

As a sustainable and carbon neutral alternative feedstock, biomass has emerged as a promising resource for green hydrogen production (Ahmed et al., 2012; Cao et al., 2020; Parthasarathy & Narayanan, 2014; Sikarwar et al., 2016; U.S. Department of Energy, 2023; Zhao et al., 2017). Biomass gasification is typically conducted in three types of reactors: fixed-bed gasifiers, entrained-flow gasifiers, and fluidized-bed gasifiers. Despite their low capital cost and operational simplicity, both updraft and downdraft fixed-bed gasifiers suffer from severe tar formation and yield a relatively low hydrogen concentration of only 10–20% (Wang et al., 2025). Entrained-flow gasifiers can effectively suppress tar formation owing to their extremely high operating temperatures. However, they impose stringent requirements on feedstock particle size, rendering biomass pretreatment costly and technically challenging (Tezer et al., 2022). Moreover, the hydrogen concentration in entrained-flow gasification is generally limited to 25–35% (Lundgren et al., 2025). At present, circulating fluidized-bed gasifiers are considered as one of the most promising reactor configurations for biomass gasification due to their excellent heat and mass transfer, uniform temperature distribution, and high fuel flexibility. Nevertheless, even under steam gasification conditions, the hydrogen concentration in the produced syngas is typically below 40%. Since most downstream chemical synthesis processes require a syngas H_2:CO_x ratio exceeding 2, extensive syngas conditioning and energy-intensive separation steps are required to enrich hydrogen, significantly increasing system complexity and cost and thereby reducing the overall competitiveness of biomass-derived hydrogen (Andersson & Lundgren, 2014; Puig-Gamero et al., 2018; Richardson et al., 2012).

In contrast, sorption-enhanced steam gasification (SESG) has emerged as a promising route for producing hydrogen or hydrogen-rich syngas by integrating biomass gasification, the water–gas shift reaction, and *in-situ* CO_2 capture in a single process step (Acharya et al., 2009; Chen & He, 2011; Parvez et al., 2021). Continuous removal of CO_2 during gasification shifts the reaction equilibrium toward H_2 formation, enabling significantly enhanced hydrogen concentrations and tunable H_2/CO_x ratios through operating conditions, which facilitates direct integration with downstream chemical synthesis processes (AlNouss et al., 2022; Broda et al., 2012; Dang et al., 2020; Fermoso et al., 2012; Gil et al., 2016; Sikarwar et al., 2022; Wu et al., 2012; Yan et al., 2020; Yang et al., 2021). Despite these advantages, the practical deployment of SESG is severely constrained by the rapid degradation of conventional CO_2 sorbents as well as the large temperature swing needed for the high-temperature and endothermic sorbent regeneration step (Jiang et al., 2017; Li et al., 2021). CaO-based sorbents typically suffer a 50–80% loss in CO_2 capacity within several tens of carbonation–decarbonation cycles due to sintering, leading to enlarged reactor size, reduced hydrogen purity, and unfavorable process economics (Abanades, 2002; Daud et al., 2016; Grasa & Abanades, 2006; Jiang et al., 2017). Although the incorporation of inert stabilizers such as Al_2O_3 or ZrO_2 can mitigate sintering, it inevitably sacrifices the overall sorption capacity (Armutlulu et al., 2017; Dang et al., 2021; Dang et al., 2016; Radfarnia & Iliuta, 2014; Rusten et al., 2007; Wu et al., 2012).

To address these limitations, a novel class of redox-activated CO_2 sorbents based on mixed-metal oxides ($A_xB_yO_z$) has been proposed (Dang et al., 2018; Li et al., 2023). In these materials, alkali or alkaline-earth A-site species capture CO_2, while transition-metal B-site species provide redox activity and catalytic functionality. During SESG, lattice oxygen donation and CO_2 capture occur simultaneously, whereas regeneration proceeds through carbonate decomposition and reformation of the mixed oxide phase. Such fully reversible phase transitions have been demonstrated to suppress sintering and enhance long-term stability (Brody et al., 2022, 2025; Dang et al., 2018). Moreover, by tailoring the elemental composition, the oxygen chemical potential can be adjusted to enable isothermal operation at 850 °C, eliminating the need for large temperature swings during regeneration (Dou et al., 2016; House et al., 2009; Masoudi Soltani et al., 2021; Wang et al., 2021). This feature is particularly attractive, as isothermal operations above 800 °C is highly desirable for efficient biomass gasification and tar suppression (Fuchs et al., 2019; Virginie et al., 2012).

In our previous study, $SrMnO_3$ was identified as an effective redox-activated CO_2 sorbent for sorption-enhanced reforming of methane and gasification of woody biomass (Cai et al., 2024). Building upon these results, the present work further explores the fuel flexibility, torrefaction effects, and long-term stability of $SrMnO_3$ using four different biomass feedstocks in a batch-scale fluidized-bed reactor. Four biomass waste feedstocks, including untreated and chemically treated materials as well as their torrefied samples, were evaluated. All untorrefied feedstocks produced hydrogen-rich syngas with H_2 purity exceeding 60% and H_2/CO ratios above 4 under isothermal operation at 850 °C. Long-term experiments in both a fluidized-bed reactor and thermogravimetric analysis (TGA), combined with comprehensive material characterization, demonstrated excellent cyclic stability of $SrMnO_3$ with stable hydrogen production, sustained CO_2 sorption capacity, and strong resistance to biomass ash, and robust structural and compositional properties. Process simulation further indicated that SESG significantly improves syngas quality with comparable heat requirements compared to the conventional indirect biomass gasification condition.

2. Methodology

2.1. Materials and characterization

The $SrMnO_3$ redox-activated CO_2 sorbents were synthesized via a solid-state reaction method. Stoichiometric amounts of $SrCO_3$ (Sigma-

Aldrich, >99.9%) and MnO_2 (Materion, >99.9%) were loaded into a 100 mL Teflon jar and ball-milled at 250 rpm for 12 h using a planetary ball mill (Columbia International, CIT-XBM4X-2.0 L). Yttria-stabilized ZrO_2 beads were employed as the milling media with a bead-to-precursor mass ratio of 5:1. To enhance mixing uniformity and reduce particle size, ethanol (Fisher Scientific, CDA 19, histological grade) was added at a dosage of 1 mL per gram of precursor. Three bead diameters (3, 6, and 10 mm) with equal mass fractions were used to improve milling efficiency.

The resulting wet slurry was dried in an oven at 95 °C for 30 min followed by 130 °C for an additional 30 min to remove residual ethanol. After drying, the powders were separated from the ZrO_2 beads, pelletized under a uniaxial pressure of 20 tons, and subsequently calcined in a muffle furnace (KSL-1200X, MTI Corporation) at 1100 °C for 10 h to form the perovskite phase. The heating and cooling ramp rates were both set to 3 °C/min. The as-prepared perovskite sorbents were sieved into two particle-size fractions: 180–425 μm for reactor experiments and <180 μm for X-ray diffraction (XRD) and X-ray Fluorescence (XRF) characterization.

The phase structures of the fresh and spent sorbents were characterized using a PANalytical X'Pert PRO X-ray diffractometer operated at 45 kV and 40 mA. Diffraction patterns were collected over a 2θ range of 15–65° with a step size of 0.0262° and a dwell time of 0.2 s per step. Phase identification and analysis were performed using Highscore Plus software.

The specific surface area and pore volume of the fresh and long-term tested samples were determined by nitrogen adsorption–desorption measurements performed on a Micromeritics ASAP 2020 analyzer at 77 K. Prior to analysis, each sample was degassed under vacuum (pressure <5 mm Hg) at 200 °C for 10 h to eliminate adsorbed gases and impurities. The surface area was evaluated using the multipoint BET method over a relative pressure range of P/P_0 = 0–0.2 providing detailed insights into the materials' surface and textural characteristics. Due to the relatively low surface area of the samples, the N_2 adsorption isotherms at 77 K exhibited a downward trend beyond P/P0 = 0.25, preventing reliable mesopore analysis using the BJH method. Therefore, the pore size distribution was instead estimated using the DFT method, focusing primarily on the micropore region.

The bulk elemental compositions of the sorbents were characterized by XRF using a Supermini 200 sequential benchtop WDXRF spectrometer (Rigaku, Japan), equipped with a 50 kV, 200 W Pd anode X ray tube, scintillation and flow proportional (F-PC) detectors. Approximately 3 g of dried powder was used for each measurement. The microscale surface morphology and elemental distribution were characterized using the Scanning Electron Microscope-Energy Dispersive X-ray Spectroscopy (SEM-EDS). The analyses were performed on a Hitachi SU8700 field-emission SEM operated at an accelerating voltage of 15 kV. During imaging, the analyzer tension was set to 2.00 kV, with a spot size of 30 and a working distance maintained between 4 and 5 mm.

To evaluate the SESG performance of $SrMnO_3$ with respect to biomass composition, four types of biomass wastes were used in this study. Untreated Southern Yellow Pine was selected as the reference feedstock. In addition, three chemically treated biomass materials were investigated: railroad ties treated with Creosote, FlamePro wood subjected to flame-retardant treatment, and decay-resistant wood treated with copper azole type C for marine applications. These materials are hereafter referred to as Pine, Creosote, FlamePro, and CuAz, respectively. Torrefaction is a mild thermal pretreatment known to dehydrate biomass and increase its C/H and C/O ratios, thereby enhancing the heating value of both the feedstock and the resulting syngas. Accordingly, Pine, FlamePro, and CuAz were torrefied at 200 °C for 20 min and are denoted as torrefied Pine, torrefied FlamePro, and torrefied CuAz, respectively.

2.2. Reactivity evaluation

Proximate analyses of the biomass wastes were performed using a TGA-55 thermogravimetric analyzer (TA Instruments). Moisture content was determined by heating the samples from room temperature to 105 °C at a rate of 15 °C/min and holding at 105 °C for 10 min under a nitrogen atmosphere. Subsequently, the samples were heated from 105 to 900 °C at 15 °C/min and maintained at 900 °C for an additional 10 min to quantify the volatile matter. The atmosphere was then switched to air to determine the fixed carbon and ash contents. The higher heating values (HHVs) of the biomass samples were measured using a Parr Model 1108 oxygen bomb calorimeter. Ultimate analyses were conducted using a CE440 CHN elemental analyzer (Exeter Analytical). The key biomass properties obtained from proximate and ultimate analyses are summarized in Table 1.

The cyclic CO_2 sorption behavior of the $SrMnO_3$ sorbents was investigated using an SDT Q650 simultaneous thermal analyzer (TA Instruments). To replicate the sorption-enhanced gasification environment, a four-step cycling protocol was implemented, comprising reduction, regeneration, and two intermediate argon purging stages separating each half-cycle. ~23 mg of fresh sorbent particles (180–425 μm) was placed in the TGA sample crucible and heated to 850 °C at a rate of 30 °C/min under an Ar flow of 140 sccm (Airgas, UHP 5.0). All gas flow rates were precisely regulated using Alicat MC-series mass flow controllers. After reaching the target temperature, the sample was equilibrated under Ar for 8 min to ensure thermal stability. The reduction–sorption step was then initiated by introducing a mixed gas stream containing 40 sccm H_2 (Airgas, UHP 5.0) and 20 sccm CO_2 (Airgas, 4.0 grade) for 40 min. Following the reduction stage, H_2 and CO_2 feeds were discontinued and the system was purged with Ar for 8 min, during which partial carbonate decomposition occurred. Regeneration was subsequently performed by supplying 35 sccm of O_2 (20 vol% in balance Ar gas) for 30 min. During this period, the reduced sorbent underwent reoxidation with substantial CO_2 release. Completion of the regeneration step marked the end of one full cycle, after which the subsequent cycle was carried out under identical conditions. A total of 30 consecutive cycles were conducted to evaluate the long-term stability of the $SrMnO_3$ sorbents. The sorption capacity was defined as the ratio between the experimentally measured moles of CO_2 release and the theoretical CO_2 uptake determined by the stoichiometric content of A-site cations. Detailed calculation methods are reported in our previous work (Cai et al., 2024).

The sorption-enhanced gasification performance of $SrMnO_3$ was evaluated in a laboratory-scale bubbling fluidized-bed (BFB) reactor. As illustrated in Fig. 1, the reactor consisted of a vertical 316 L stainless-steel tube (25.4 mm OD, 23.6 mm ID) placed in a tubular furnace (MTI OTF-1200X-S-VT) with an effective heating length of approximately 20 cm. The reaction temperature was monitored using an S-type thermocouple positioned at the center of the heating zone. Prior to each experiment, a layer of 16-mesh Al_2O_3 particles (~1.2 mm) was loaded at the bottom of the reactor to support the bed, followed by 15 g of $SrMnO_3$, corresponding to a close-packed bed height of ~2 cm.

A four-step cyclic operation was employed, consisting of reduction, regeneration, and two intermediate purge steps. During the reduction and purge stages, 923 sccm of Ar (Airgas, UHP 5.0) was supplied, while regeneration was carried out using a mixture of Ar and O_2 (683/240 sccm). All gas flow rates were controlled using mass flow controllers (Brooks 5850 E series). Steam was generated by injecting deionized water into the heated zone through a stainless-steel tube (3.18 mm OD, 2.16 mm ID) using a syringe pump (Harvard Apparatus) at a rate of 0.21 mL/min, corresponding to 277 sccm steam and a steam-to-gas ratio of 0.3. The Sauter-mean particle size of the $SrMnO_3$ sorbent was approximately 320 μm. The minimum fluidization velocity estimated

Table 1
Proximate and ultimate analysis of biomass used in experiments.

Item	HHV_{ar}[a]	M_{ar}	A_{ar}	V_{ar}	FC_{ar}	C_{daf}	H_{daf}	O_{daf}[b]	N_{daf}
	MJ/kg	%	%	%	%	%	%	%	%
Pine	16.92	6.00	0.81	78.63	14.56	50.0	6.20	43.7	0.10
Creosote	18.39	4.02	1.86	84.41	9.66	49.6	5.7	44.6	0.10
FlamePro	17.05	4.61	5.70	64.86	24.84	46.9	6.0	46.6	0.60
CuAz	17.14	5.24	1.69	79.54	13.20	50.9	5.9	43.1	0.06
Torrefied Pine	20.25	4.07	1.55	76.45	17.93	54.3	5.9	39.9	0.00
Torrefied FlamePro	22.46	3.82	3.79	47.70	44.69	64.4	4.9	29.7	0.90
Torrefied CuAz	18.66	3.74	1.56	78.61	16.1	51.0	5.5	43.5	0.02

Note.
[a] as received samples.
[b] dried ash-free samples.

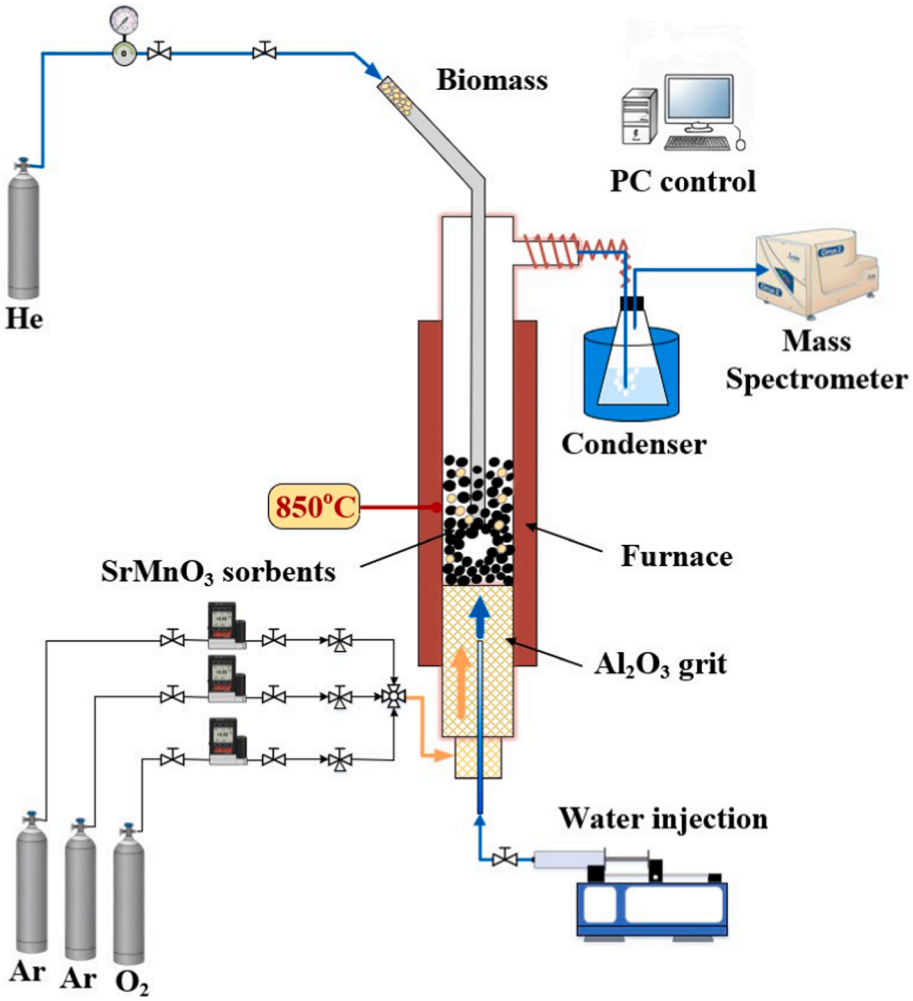

Fig. 1. Schematic diagram of the batch fluidized bed reactor for SESG of biomass.

from the Ergun equation was approximately 0.03 m/s under the Ar atmosphere, whereas the superficial gas velocity used in the fluidized-bed experiments was approximately 0.19 m/s. Therefore, the operating velocity was more than six times U_{mf}, suggesting that the bed was maintained under the fluidized conditions. The product gas stream was heat-traced and passed through an ice-cooled condenser to remove water before on-line analysis using an MKS Cirrus II quadrupole mass spectrometer. The mass spectrometer was calibrated using standard gases after the experiments. The gas compositions are reported on a dry and Ar-free basis for each cycle.

Biomass particles (200–500 μm) were injected via a stainless-steel injection tube (3.75 mm OD, 3.35 mm ID) inserted into the sorbent bed to enhance mixing. A pulse-feeding mode was adopted, in which 0.3 or 0.1 g of biomass was injected per pulse using ~3 mL of helium gas at 20 psig as the carrier gas. Two consecutive pulses were applied to minimize biomass retention in the feed line. For each biomass type, at least three effective cycles were conducted with five biomass pulses per cycle. Additional experiments involving deep reduction (12 pulses per cycle) and extended operation over 10 cycles were performed to assess the effect of reduction extent and the long-term stability of $SrMnO_3$. The CO_2 sorption capacity was calculated based on the CO_2 released in the regeneration step. The cold gas efficiency (CGE) of syngas was

calculated using Eq. (1),

$$\eta_{CGE} = \frac{\sum Q_i \times LHV_i}{m_{fuel} \times LHV_{fuel}} \times 100\% \quad (1)$$

Where Q_i is the gas volume (Nm^3) of a specific syngas component (H_2, CO, and CH_4), LHV_i is its lower heating value (kJ/Nm^3), Q_{fuel} is the mass of injected biomass fuel (g), and LHV_{syngas} is the lower heating value of the biomass fuel (kJ/g).

2.3. Process modeling

Aspen Plus was used to compare conventional indirect biomass gasification (base case, adapted from Dutta et al. NREL (Dutta et al., 2011) and $SrMnO_3$-based SESG. The simplified process schematics are presented in Fig. 2, while the corresponding Aspen Plus flowsheets for each configuration are shown in Supplementary Fig. S1. Details of the simulation methodology are also provided in the Supporting Information. We note that the modeling effort is a scenario-level thermodynamic comparison based on bench-scale experimental data, intended to illustrate the directional process advantages of SESG rather than providing a fully optimized design. We further acknowledge that the results are sensitive to feedstock composition, reactor configuration, and heat-integration assumptions.

Both cases use the same biomass feedstock (untreated Southern Yellow Pine, 10,000 kg/h dry basis, 49.5 MW_{th} LHV) and the same biomass decomposition step, and the comparison is drawn at the gasifier plus char combustor for the base case, and gasifier plus regenerator for SESG. The base case gasifier was operated at 868 °C with S/B = 0.4 and olivine as the heat carrier, following the NREL methodology. The SESG gasifier was operated at 850 °C with a C/steam molar ratio of 1:2, matching our fluidized-bed experiments.

Because $SrMnO_3$ is not a defined component in the Aspen Plus databank, the sorbent was not looped explicitly. Instead, an O_2 donation stream into the gasifier represented oxygen transfer from the sorbent, with its flowrate tuned to match the experimental syngas LHV. As observed experimentally, $SrMnO_3$ returns to its original state at the end of each cycle, so by Hess's law the sorbent reactions in the gasifier (reduction + carbonation) and regenerator (oxidation + decarbonation) are captured collectively in the gasifier-regenerator pair heat duty, regardless of whether the sorbent is tracked as an explicit stream. Both reactors operate isothermally at 850 °C, so the sorbent carries no sensible-heat penalty between them. In addition to the five-pulse case (135 kmol/h O_2 donation), a four-pulse case was modeled to represent partial sorbent regeneration with reduced oxygen donation (85 kmol/h), analogous to partial-oxidation operation in a CFB configuration. The 4-pulse case represents a hypothetical partial-regeneration scenario, indicating the upper-bound performance achievable under optimized CFB operation, while the 5-pulse case reflects the integrated experimental performance of the current batch fluidized-bed configuration. Complete flowsheets, stream-level data, and detailed assumptions are provided in the appendix (Fig. S1, Table S3 and S4).

3. Results and discussion

3.1. Comparison of different biomass feedstock

The effect of biomass injection amount was first investigated using as-received pine wood as the feedstock. For a small pulse injection of 0.1 g/pulse, negligible H_2 production was observed until the fifth pulse injection (Fig. S2a), indicating that the *in-situ* CO_2 sorption and reforming reactions were insufficient to establish a hydrogen-rich environment during the initial cycles due to the complete oxidation of the biomass by the lattice oxygen in $SrMnO_3$. This behavior is consistent with our previous findings, as $SrMnO_3$ requires an initial reduction step before active SrO species are released to capture CO_2 (Brody et al., 2025). In contrast, when the pulse injection amount was increased to 0.3 g, H_2 generation was initiated as early as the second pulse injection, and the H_2 purity exceeded 70% from the fourth injection (Fig. S2b). As shown in Fig. 3(a) and (b), an extended operation with 12 consecutive biomass pulses (0.3 g each) was subsequently performed to evaluate effectiveness of sorbent. The H_2 purity reached a maximum of 75% at the fourth injection and then gradually declined to below 60% in the later cycles. Meanwhile, the total volume of combustible components (H_2, CO, and CH_4) in the syngas decreased progressively, accompanied by an increase in CO_2 concentration to approximately 23%. This trend suggests a gradual depletion of the sorption-enhancement effect of the $SrMnO_3$ sorbent, as its CO_2 uptake capacity became saturated over repeated injections. During the regeneration step, the released CO_2 corresponded to approximately 65 mol% of the theoretical sorption capacity of $SrMnO_3$ (~24 wt%), demonstrating a substantial CO_2 uptake. Such a high utilization of sorption capacity confirms the effectiveness of $SrMnO_3$ for isothermal SESG of biomass, enabling significant *in-situ* CO_2 removal and thereby promoting hydrogen enrichment in the product gas.

As presented in Fig. 3(c) and (d), SESG performance was evaluated for four untorrefied biomass samples. All four feedstocks produced syngas with H_2 purity exceeding 60% and an H_2/CO ratio higher than 4, which was sufficient for downstream chemical synthesis processes, such as methanol or methane production. Among them, untreated pine exhibited the highest H_2 purity, followed by CuAz, FlamePro, and Creosote. In contrast, Creosote showed the highest total syngas yield, with the average CGE of the last three injections reaching 107%. The CGE exceeding 100% is attributed to the external furnace heat input, which was not included in the CGE denominator. During char steam gasification ($C + H_2O \rightarrow CO + H_2$), part of this external heat input is converted into the chemical energy of CO and H_2, resulting in an apparent CGE above 100%. FlamePro, however, exhibited significantly lower syngas production compared to the other samples, with an average CGE of only 68% over the last three injections.

Although the carbon content of all four biomass samples was similar

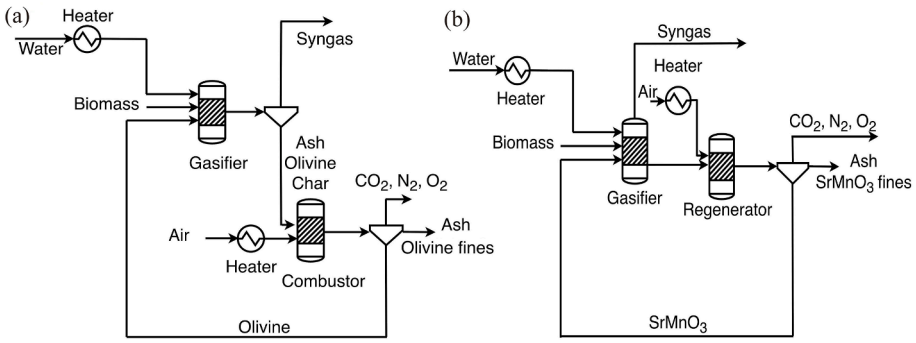

Fig. 2. Simplified flow diagrams for: (a) indirect biomass gasification (b) SESG of biomass with $SrMnO_3$ sorbents.

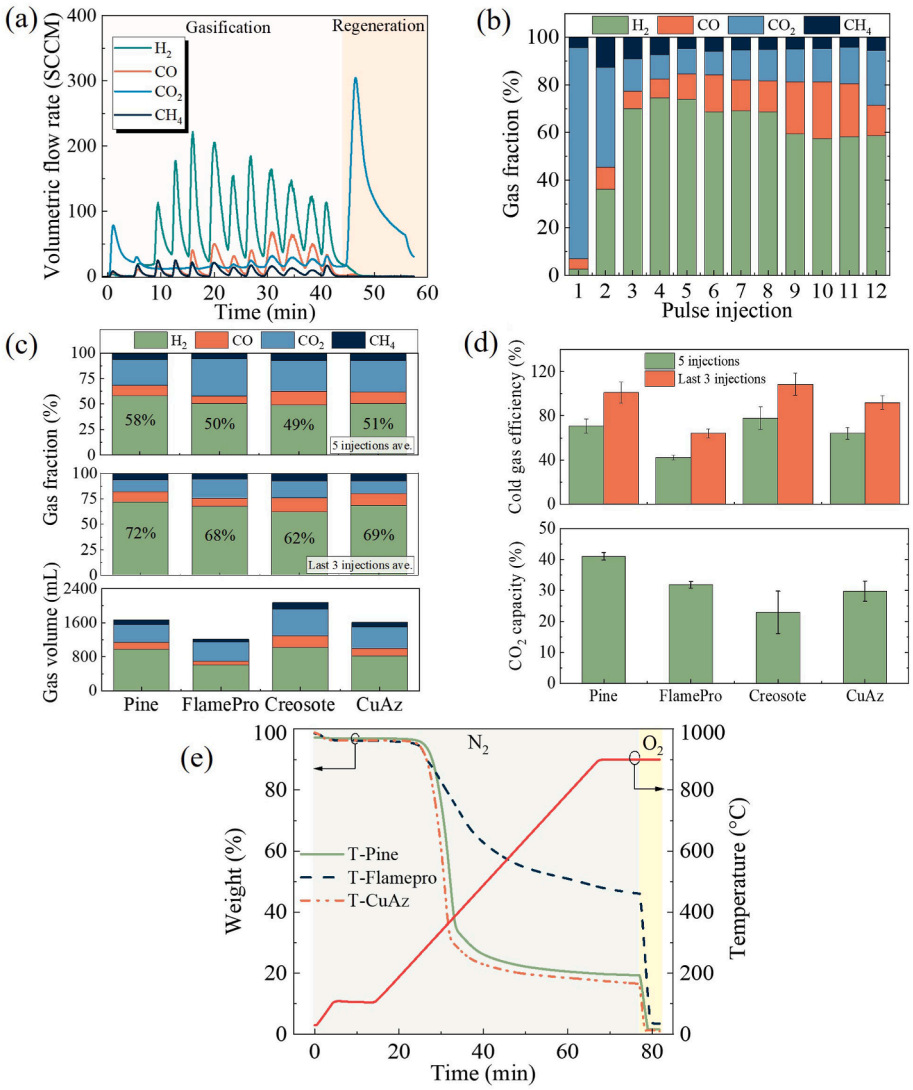

Fig. 3. SESG performance of different biomass feedstocks in the fluidized bed reactor: (a) gas evolution profiles and (b) gas composition during extended operation with 12 consecutive pulses of untorrefied pine; (c) total syngas yield and average gas concentrations; and (d) cold gas efficiency and CO_2 sorption capacity for different biomass feedstocks; (e) reaction properties of different biomass feedstocks in the TGA.

(approximately 50%), their volatile matter and fixed carbon contents differed substantially. As listed in Table 1, Creosote exhibited the highest volatile matter content (84%), followed by Pine and CuAz (both ~79%), while FlamePro contained only 65%. This trend was consistent with the observed CGEs. Moreover, as shown in Fig. 3(e), the devolatilization behaviors of Pine, Creosote, and CuAz were relatively similar, occurring primarily around 300 °C and resulting in approximately 70% weight loss. In contrast, FlamePro exhibited remarkedly different behavior, with only about 30% weight loss within the same temperature range. Rapid devolatilization generates a larger fraction of reactive gaseous intermediates, which can readily contact the sorbent particles and promote effective sorption-enhanced reactions. In comparison, char-dominated reactions proceed more slowly and are governed by limited gas–solid or solid–solid interactions, resulting in lower overall carbon conversion efficiency. Consequently, the syngas performance of FlamePro was significantly inferior to that of the other three biomass feedstocks. Regarding tar formation, while not precisely quantified in this small-scale study, visual observation indicated no obvious tar formation for Pine, FlamePro, and CuAz. However, Creosote resulted in visible dark oily deposition on the downstream PTFE tubing, which was consistent with its high volatile content. It should be noted that the biomass feeding amount was relatively small in this study, with 1.5 g per cycle, which limited reliable tar collection and quantitative analysis. Therefore, the present results only provide a qualitative indication of tar formation. Quantitative tar measurements under larger feeding rates are needed in future work to further evaluate tar formation and suppression across different feedstocks.

Regarding CO_2 sorption capacity, the carbonation reaction is generally slower than devolatilization. For Creosote, the substantial and rapid release of CO_2 during devolatilization likely exceeded the instantaneous sorption kinetics and available active sites of the sorbent, leading to partial CO_2 escape. This explains the comparatively lower H_2 concentration and incomplete utilization of CO_2 sorption capacity observed for Creosote, despite its higher syngas yield.

It should also be noted that the sorbent bed height in this study was limited to only approximately 2 cm under the closed-packing condition prior to fluidization. In practical fluidized-bed systems, performance could be further enhanced by improving gas-solid contact between biomass-derived gases and sorbent particles or by extending the effective residence time within the sorbent bed, thereby facilitating more complete CO_2 capture and hydrogen enrichment. Additionally, by adjusting the regeneration duration, the oxidation state of $SrMnO_3$ and the corresponding lattice oxygen donation capacity of the sorbent can be effectively tuned. This partial regeneration approach can mitigate over-

oxidation of syngas during the initial pulses and improve the overall hydrogen purity.

3.2. Impact of torrefaction

Generally, torrefaction pretreatment removes hydroxyl groups and moisture, reduces volatile matter content, and increases the C/H and C/O ratios of biomass. As listed in Table 1, the volatile matter content decreased for all three biomass samples after torrefaction, most notably for the FlamePro sample, where it declined from 65% to 48%. Correspondingly, the C/H and C/O ratios, as well as the higher heating values, increased significantly. However, as shown in Fig. 4(a) and (b), the H_2 purity of all torrefied samples decreased markedly, with the most pronounced reduction observed for FlamePro, where H_2 purity dropped from 68% to 41%. The total syngas yields also decreased substantially after torrefaction. This behavior can be attributed to the altered devolatilization and char formation characteristics induced by torrefaction. As shown in Fig. 4(c), the rapid devolatilization stage almost completely disappeared for the torrefied FlamePro biomass, resulting in a much lower release rate of reactive gaseous species. The devolatilization stage typically provides superior contact between reactive gases and sorbent particles, facilitating rapid gas-solid reactions and more effective sorption-enhanced gasification. In contrast, torrefaction increases the fixed carbon fraction, shifting the conversion pathway toward char-dominated reactions. In the current batch reactor configuration, which lacks particle separation and recycling systems, char particles, due to their lower density and smaller size, are prone to elutriation before achieving complete conversion. Furthermore, the relatively slow kinetics of char–sorbent interactions and steam gasification of char further limit overall carbon conversion efficiency. As a result, both the total carbon conversion and the effective CO_2 sorption capacity decreased after torrefaction.

The torrefaction experiments indicated that SESG can directly achieve H_2 enrichment without relying on a torrefaction-based pretreatment step. A high volatile matter also benefits the syngas quality. Additionally, the fluidized bed configuration provides greater fuel flexibility, enabling the elimination of complex biomass pretreatment procedures. For practical applications, the implementation of a carbon stripper and cyclone separator would help ensure sufficient fuel particle residence time and improve char conversion efficiency, thereby further enhancing overall carbon balance and sorption-enhanced performance.

3.3. Long-term stability

As shown in Fig. 5(a), the $SrMnO_3$ sorbents were first reduced and exposed to CO_2, resulting in a pronounced weight gain due to CO_2 uptake during the reduction stage. After switching to an oxidizing atmosphere, the sorbents were regenerated and released the absorbed CO_2, leading to a significant weight loss. The cyclic weight variation clearly demonstrates the reversible redox-activated sorption behavior of the sorbent material.

Long-term stability is a critical parameter for the SESG process. Conventional CaO-based sorbents typically suffer from severe sintering during repeated carbonation-calcination cycles (Dunstan et al., 2021), which leads to progressive deactivation and a decline in H_2 purity during operation. In contrast, no evident deactivation in CO_2 sorption capacity was observed for the $SrMnO_3$ sorbent. After several initial cycles, the CO_2 uptake stabilized at approximately 42 mol% and gradually increased to around 53 mol%. During the cyclic test, the maximum weight after the H_2/CO_2 reduction/carbonation stage remained nearly constant, indicating that the sorbent was close to CO_2 saturation in each cycle (Fig. S3). Therefore, the apparent increase in reversible CO_2 capacity from approximately 42 to 53 mol% was mainly caused by the larger weight loss during regeneration, suggesting more complete CO_2 release in later

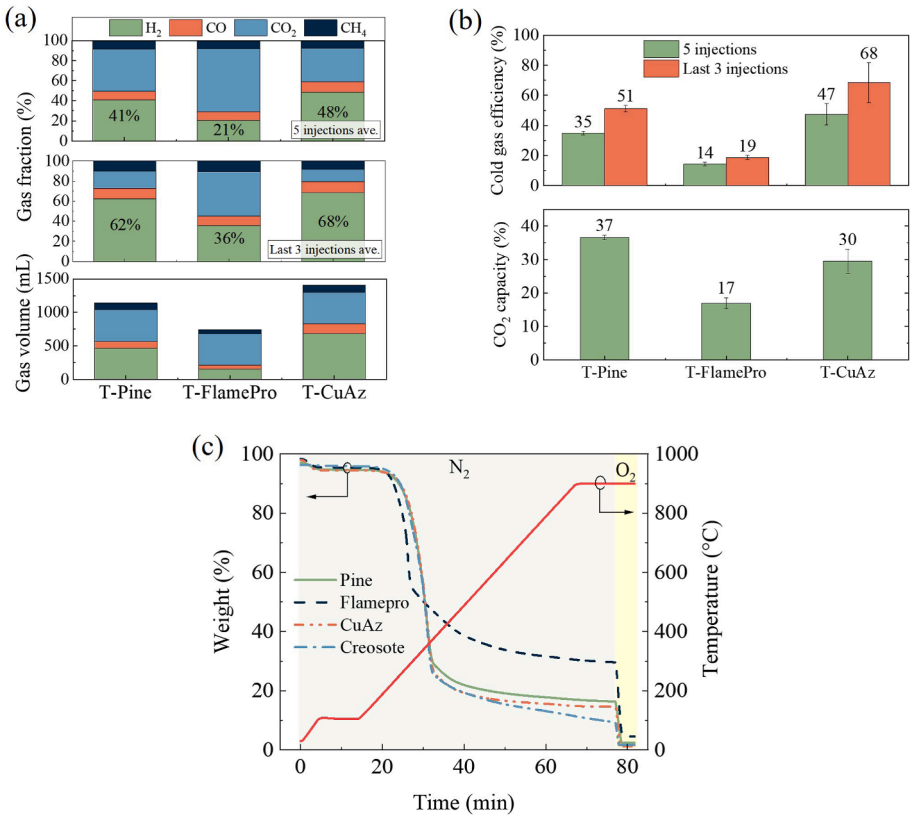

Fig. 4. SESG performance of different torrefied biomass feedstocks in the fluidized bed: (a) total syngas yield and average gas concentrations; and (b) cold gas efficiency and CO_2 sorption capacity; (c) reaction properties of different torrefied biomass feedstocks in the TGA.

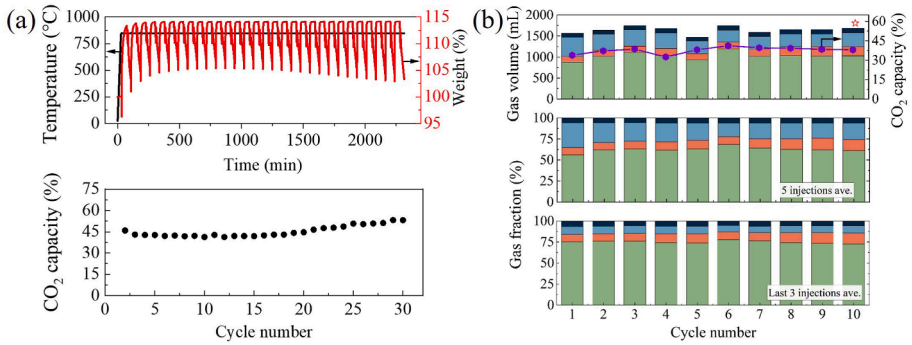

Fig. 5. Long-term stability of $SrMnO_3$ sorbents for SESG of untorrefied pine: (a) performance evaluated using a TGA; and (b) performance tested in a batch fluidized-bed reactor (the red star in the final cycle indicates a more complete regeneration condition with an extended regeneration time).

cycles, rather than a continuous increase in the maximum CO_2 uptake. This improvement in reaction kinetics is likely associated with structural evolution of $SrMnO_3$ during cyclic operation, which significantly differs from the sintering-driven deactivation observed in conventional CaO-based sorbents. To further evaluate the effect of ash on cyclic stability, 10 wt% untorrefied pine ash was introduced into the $SrMnO_3$ sorbent. In practical chemical looping reactors, such a high ash-to-sorbent ratio is unlikely to occur with proper ash separation and solid management. Therefore, this experiment was designed as a preliminary stress test to examine the cyclic redox–sorption stability of $SrMnO_3$ under a selected high-ash condition. The CO_2 sorption capacities over nine cycles remained nearly constant (Fig. S4). The sorption capacity in the final cycle reached 47 mol%, corresponding to a theoretical value of 52 mol% for the active sorbent phase, which was even higher than the 49 mol% observed for the ash-free case. These results suggest that $SrMnO_3$ maintained stable cyclic behavior under the tested pine-ash condition. It should be noted that chemically treated waste may contain additional species, such as Cu-, halogen-, and preservative-derived compounds, which could interact differently with the sorbent and require further systematic investigation. These effects were beyond the scope of the present work.

As shown in Fig. 5(b), the long-term performance was further validated in a batch fluidized-bed reactor. Both H_2 purity and CO_2 sorption capacity remained stable during cyclic operation, demonstrating that $SrMnO_3$ enables stable isothermal SESG performance in a fluidized-bed configuration. The average H_2 purity over the last three cycles exceeded 70%, while the CO_2 sorption capacity stabilized at approximately 38–40 mol%. Owing to kinetic limitations, complete regeneration could not be achieved within the standard cycle time. Therefore, in the tenth cycle, the oxidation (regeneration) period was intentionally extended, resulting in a CO_2 capacity of approximately 60 mol%, confirming the ability to achieve higher theoretical capacity under a more complete regeneration condition.

XRF analysis of the fresh and regenerated samples showed that the bulk composition of the regenerated sample remained nearly unchanged compared to the fresh sample (table S2). The detected Fe_2O_3 and Cr_2O_3 likely originated from the reactor wall, as a 316 L stainless steel tube was used. This issue could be mitigated by employing more temperature-resistant materials (e.g., 310 S stainless steel). As shown in Fig. 6(a and b), the fresh $SrMnO_3$ sample exhibited a dense microstructure with negligible visible porosity due to high-temperature calcination during synthesis. However, the sorbent developed a more roughened and sponge-like surface morphology after ten cycles of operation. The BET surface area remained nearly unchanged after cycling, increasing slightly from 2.40 to 2.47 m^2/g. In contrast, the pore size distribution of the cycled $SrMnO_3$ sample revealed the emergence of a dominant micropore population centered at approximately 1.25 nm, which was absent in the fresh sample (Fig. S5). The repeated absorption and release of CO_2 induced structural evolution, generating a more open framework that likely contributed to the enhanced reaction kinetics observed in later cycles. SEM-EDS analysis further revealed uniform elemental distribution in both fresh and spent samples, with no detectable elemental segregation. As shown in Fig. 6(c and d), XRD analysis showed that the $SrMnO_3$ phase remained dominant in the regenerated samples, with only minor amounts of $SrCO_3$, MnO_2, and Sr_3MnO_7 detected. It is expected that a longer regeneration time could further promote CO_2 release and enable more complete recovery of the $SrMnO_3$ phase. These results indicate robust chemical and structural stability of $SrMnO_3$ during prolonged redox–sorption cycling.

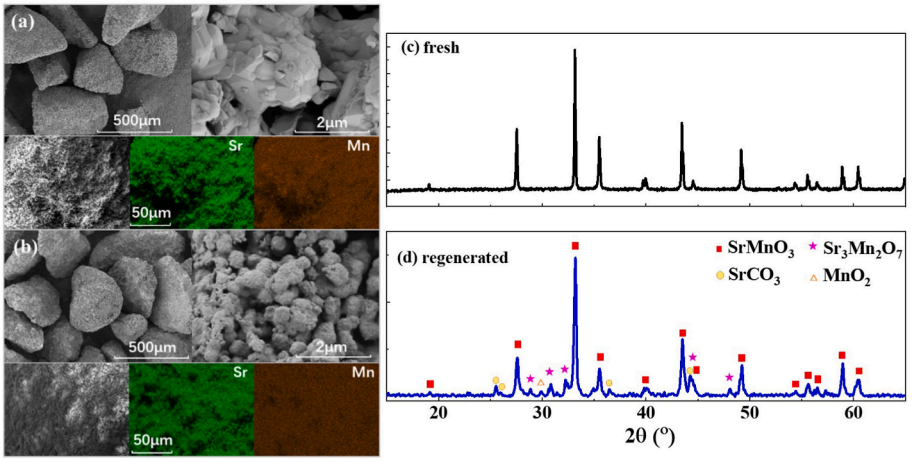

Fig. 6. SEM–EDS images of $SrMnO_3$ sorbents, including (a) fresh and (b) regenerated samples after long-term fluidized-bed operation; corresponding XRD patterns are shown in (c) and (d).

3.4. Simulation of gasifier performance

As listed in Table 2, the indirect steam gasifier (base case), consisting of a gasification step and a char combustion step, was net exothermic with a heat release of −3.09 MW. Here, negative heat-demand values denote net heat release from the system (i.e., recoverable surplus heat available for integration with downstream operations or steam generation), while positive values denote a net heat input requirement. The feedstock preheating duties, including steam preheating from 150 °C to 600 °C and air preheating from 25 °C to 600 °C, required 2.39 MW and 1.11 MW, respectively. Here, we assumed that the downstream operations such as a methanation or methanol synthesis step generated enough low-grade heat to produce steam at 150 °C. In addition, heat recovery from the syngas product and flue gas streams amounted to −5.28 MW and −3.86 MW, respectively, when cooled to 150 °C, resulting in −8.71 MW surplus for heat integration.

Moreover, two cases were considered for SESG. In the first case, the overall syngas yields from all five pulses were taken into consideration. In the second case, the syngas yields from four pulses, i.e., pulses 2–5, were used to determine gasifier performance when partial sorbent regeneration was implemented in a CFB-based SESG. In the 5-pulse case, the gasifier-regenerator pair heat demand was net exothermic with a release of −3.60 MW_{th}, as both steam for gasifier and air for regenerator were preheated to 600 °C. The feedstock preheating duties, including steam preheating from 150 °C to 600 °C and air preheating from 25 °C to 600 °C, required 3.57 MW and 3.13 MW, respectively. Heat recovery from the syngas and CO_2-containing stream and the regenerator flue gas stream amounted to −10.71 MW and −3.96 MW, respectively, when cooled to 150 °C, resulting in −11.57 MW available for heat incorporation. Conversely, the four-pulse scenario demonstrated that while the heat-balance framework remained similar, overall heat availability for integration decreased significantly to −4.58 MW. In this case, the gasifier-regenerator system transitioned to endothermic operation because of reduced oxygen consumption, modeled to mimic partial oxidation.

Comparative performance analysis based on raw experimental data from the unoptimized lab-scale fluidized bed revealed that the SESG process (five-pulse case) achieved a cold gas efficiency of 72.4%, comparable to the 73% efficiency of indirect steam gasification. However, the SESG configuration realized a hydrogen mass yield approximately 4.8 times higher. Partial sorbent regeneration in the CFB reactor (four-pulse case) further demonstrated the process optimization potential, indicating achievable cold gas efficiencies of 85.8% alongside a 5.9-fold increase in hydrogen mass yield compared to base case. Furthermore, the resulting syngas composition is demonstrably superior for downstream catalytic conversion into high-value chemical feedstocks or fuels, such as methane, methanol, and Fischer-Tropsch liquids. For a downstream methanol or Fischer–Tropsch synthesis target ($H_2/CO \approx 2$), the indirect gasification pathway requires a dedicated water-gas-shift step, downstream CO_2 removal (typically amine or Selexol), and tar-reforming capacity. The SESG syngas already exceeds the target H_2/CO ratio and contains substantially less CO_2 and heavy hydrocarbons, so the WGS reactor can be eliminated, the CO_2-removal duty is reduced on a per-kg-H_2 basis, and tar reformer sizing is minimized. The economic consequences of these benefits are quantified in our recent TEA study (Garcia-Vallejo et al., 2025).

Table 2
Comparison of key performance metrics between conventional indirect steam gasification and SESG of biomass based on Aspen Plus modeling.

Item		Base case (indirect steam gasification)	SESG cases	
			5 pulses	4 pulses
Net pair heat demand[a] (MW_{th})		−3.07	−3.60	3.09
Net heat demand (MW_{th})		−8.71	−11.57	−4.58
Product performance (CGE)		73%	72.35%	85.80%
Syngas molar fraction	H_2	0.242	0.61	0.68
	CO	0.234	0.17	0.15
	CO_2	0.278	0.19	0.12
	CH_4	0.125	0.04	0.04
	$C_{10}H_8$	0.003	n.r.	n.r.
	C_2H_6	0.061	n.r.	n.r.
	C_2H_4	0.004	n.r.	n.r.
	C_3H_8	0.048	n.r.	n.r.
	C_6H_6	0.001	n.r.	n.r.

Note.
[a] Net pair heat demand refers to the net heat demand of the gasifier-regenerator pair (SESG cases) or the gasifier-combustor pair (base case). CGE = cold gas efficiency. n. r. = not reported (species not formed in significant amounts under SESG conditions).

4. Conclusions

This study comprehensively investigated the performance of $SrMnO_3$ redox-activated CO_2 sorbents for producing hydrogen-rich syngas in a fluidized bed for isothermal SESG of biomass. $SrMnO_3$ sorbents exhibited excellent fuel flexibility with all four untorrefied biomass producing over 60% pure H_2 and H_2/CO ratios above 4. Among these fuels, untreated pine achieved the highest H_2 purity up to 73%, followed by CuAz, FlamePro, and Creosote. Near ideal cold gas efficiencies (CGE ≈ 100%) were obtained for pine, CuAz, and creosote from the externally heated lab-scale fluidized bed, whereas FlamePro showed a lower CGE (~68%) due to its low volatile content and high fixed carbon fraction. Even though torrefaction pretreatment is commonly used to improve biomass fuel properties, the suppressed devolatilization and high char formation led to a reduced H_2 purity by 10~20%. These results also indicate that SESG can directly achieve hydrogen enrichment without the need for complex biomass pretreatment. Additionally, the $SrMnO_3$ sorbent exhibited excellent cyclic stability, with CO_2 sorption capacity stabilizing at 53 mol% in TGA without noticeable deactivation. Structural characterization by XRD, SEM-EDS, and XRF further confirmed its robust chemical and structural stability during prolonged cyclic operation. Consistent performance was also observed in fluidized-bed operation, where H_2 purity remained above 70% with stable CO_2 capacity above 38%. Process simulation showed that SESG significantly improved syngas quality, increasing H_2 content from 24% in the indirect biomass gasification to 68%, along with an increase in CGE from 73% to 86% under optimized conditions. Despite comparable heat demand, the improved syngas composition reduces downstream conditioning requirements, enabling a more integrated and efficient process. Overall, $SrMnO_3$ is a promising and robust sorbent for efficient and flexible biomass-to-hydrogen conversion under isothermal SESG conditions. Future work will focus on reactor scale-up to further validate the performance of $SrMnO_3$ and other redox-activated sorbents under practical operating conditions.

CRediT authorship contribution statement

Runxia Cai: Writing – original draft, Investigation, Formal analysis, Data curation, Conceptualization. **Mahe Rukh:** Writing – original draft, Investigation, Formal analysis, Data curation. **Andrew Jones:** Resources, Methodology, Data curation. **Leo Brody:** Investigation, Formal analysis. **Alexandra Pierce:** Data curation. **Mahdi Niknam Shahrak:** Data curation. **Stephen Kelly:** Supervision, Resources. **Sunkyu Park:** Supervision, Resources, Investigation. **Fanxing Li:** Writing – review & editing, Supervision, Investigation, Funding acquisition, Conceptualization.

Declaration of competing interest

The authors declare that they have no known competing financial interests or personal relationships that could have appeared to influence the work reported in this paper.

Acknowledgements

This work was supported by the U.S. Department of Energy Office of Energy Efficiency & Renewable Energy (no. EE0008809) and the US National Science Foundation (CBET-1923468). We acknowledge the use of the Analytical Instrumentation Facility (AIF) at North Carolina State University, which is supported by the State of North Carolina and the National Science Foundation.

Appendix A. Supplementary data

Supplementary data to this article can be found online at https://doi.org/10.1016/j.partic.2026.05.018.

References

Abanades, J. C. (2002). The maximum capture efficiency of CO2 using a carbonation/calcination cycle of CaO/$CaCO_3$. *Chemical Engineering Journal, 90*, 303–306.

Acar, C., & Dincer, I. (2020). The potential role of hydrogen as a sustainable transportation fuel to combat global warming. *International Journal of Hydrogen Energy, 45*, 3396–3406.

Acharya, B., Dutta, A., & Basu, P. (2009). Chemical looping gasification of biomass for hydrogen-enriched gas production with in-process carbon dioxide capture. *Energy & Fuels, 23*, 5077–5083.

Ahmed, T. Y., Ahmad, M. M., Yusup, S., Inayat, A., & Khan, Z. (2012). Mathematical and computational approaches for design of biomass gasification for hydrogen production: A review. *Renewable and Sustainable Energy Reviews, 16*, 2304–2315.

AlNouss, A., Shahbaz, M., McKay, G., & Al-Ansari, T. (2022). Bio-methanol production from palm wastes steam gasification with application of CaO for CO_2 capture: Techno-economic-environmental analysis. *Journal of Cleaner Production, 341*, Article 130849.

Andersson, J., & Lundgren, J. (2014). Techno-economic analysis of ammonia production via integrated biomass gasification. *Applied Energy, 130*, 484–490.

Antzaras, A. N., & Lemonidou, A. A. (2022). Recent advances on materials and processes for intensified production of blue hydrogen. *Renewable and Sustainable Energy Reviews, 155*, Article 111917.

Armutlulu, A., Naeem, M. A., Liu, H. J., Kim, S. M., Kierzkowska, A., Fedorov, A., & Muller, C. R. (2017). Multishelled CaO microspheres stabilized by atomic layer deposition of Al_2O_3 for enhanced CO_2 capture performance. *Advanced Materials, 29*, Article 1702896.

Broda, M., Kierzkowska, A. M., Baudouin, D., Imtiaz, Q., Copéret, C., & Müller, C. R. (2012). Sorbent-enhanced methane reforming over a Ni–Ca-based, bifunctional catalyst sorbent. *ACS Catalysis, 2*, 1635–1646.

Brody, L., Bekheet, M. F., Yang, K., Müller, J. T., Rukh, M., Portillo, S., Schomäcker, R., Gili, A., Gurlo, A., & Li, F. (2025). Reversible phase transitions enable cyclic isothermal CO_2 capture in redox-activated perovskite-structured sorbents. *Advanced Functional Materials, 35*.

Brody, L., Cai, R., Thornton, A., Liu, J., Yu, H., & Li, F. (2022). Perovskite-based phase transition sorbents for sorption-enhanced oxidative steam reforming of glycerol. *ACS Sustainable Chemistry & Engineering, 10*, 6434–6445.

Cai, R., Yang, K., Wang, X., Rukh, M., Bosari, A. S., Giavedoni, E., Pierce, A., Brody, L., Tang, W., Westmoreland, P. R., & Li, F. (2024). High-throughput design of complex oxides as isothermal, redox-activated CO_2 sorbents for green hydrogen generation. *Energy & Environmental Science, 17*, 6279–6290.

Cao, L., Yu, I. K. M., Xiong, X., Tsang, D. C. W., Zhang, S., Clark, J. H., Hu, C., Ng, Y. H., Shang, J., & Ok, Y. S. (2020). Biorenewable hydrogen production through biomass gasification: A review and future prospects. *Environmental Research, 186*, Article 109547.

Chen, D., & He, L. (2011). Towards an efficient hydrogen production from biomass: A review of processes and materials. *ChemCatChem, 3*, 490–511.

da Silva Veras, T., Mozer, T. S., da Costa Rubim Messeder dos Santos, D., & da Silva César, A. (2017). Hydrogen: Trends, production and characterization of the main process worldwide. *International Journal of Hydrogen Energy, 42*, 2018–2033.

Dang, C., Li, Y., Yusuf, S. M., Cao, Y., Wang, H., Yu, H., Peng, F., & Li, F. (2018). Calcium cobaltate: A phase-change catalyst for stable hydrogen production from bio-glycerol. *Energy & Environmental Science, 11*, 660–668.

Dang, C., Liu, L., Yang, G., Cai, W., Long, J., & Yu, H. (2020). Mg-promoted Ni-CaO microsphere as bi-functional catalyst for hydrogen production from sorption-enhanced steam reforming of glycerol. *Chemical Engineering Journal, 383*, Article 123204.

Dang, C., Long, J., Li, H., Cai, W., & Yu, H. (2021). Pd-promoted ni-ca-al bi-functional catalyst for integrated sorption-enhanced steam reforming of glycerol and methane reforming of carbonate. *Chemical Engineering Science, 230*.

Dang, C., Yu, H., Wang, H., Peng, F., & Yang, Y. (2016). A bi-functional Co–CaO–$Ca_{12}Al_{14}O_{33}$ catalyst for sorption-enhanced steam reforming of glycerol to high-purity hydrogen. *Chemical Engineering Journal, 286*, 329–338.

Daud, F. D. M., Vignesh, K., Sreekantan, S., & Mohamed, A. R. (2016). Improved CO_2 adsorption capacity and cyclic stability of CaO sorbents incorporated with MgO. *New Journal of Chemistry, 40*, 231–237.

Dawood, F., Anda, M., & Shafiullah, G. M. (2020). Hydrogen production for energy: An overview. *International Journal of Hydrogen Energy, 45*, 3847–3869.

Dou, B., Wang, C., Song, Y., Chen, H., Jiang, B., Yang, M., & Xu, Y. (2016). Solid sorbents for in-situ CO_2 removal during sorption-enhanced steam reforming process: A review. *Renewable and Sustainable Energy Reviews, 53*, 536–546.

Dunstan, M. T., Donat, F., Bork, A. H., Grey, C. P., & Muller, C. R. (2021). CO_2 capture at medium to high temperature using solid oxide-based sorbents: Fundamental aspects, mechanistic insights, and recent advances. *Chem Rev, 121*, 12681–12745.

Dutta, A., Talmadge, M., Hensley, J., Worley, M., Barton, D., Groendijk, P., Ferrari, D., Stears, B., Searcy, E. M., Wright, C. T., & Hess, J. R. (2011). *Process design and economics for conversion of Lignocellulosic biomass to ethanol: Thermochemical pathway by indirect gasification and mixed alcohol synthesis, NETL Technical ReportNREL/TP-5100-51400*.

Fermoso, J., Rubiera, F., & Chen, D. (2012). Sorption-enhanced catalytic steam gasification process: A direct route from lignocellulosic biomass to high purity hydrogen. *Energy & Environmental Science, 5*, 6358.

Fuchs, J., Schmid, J. C., Müller, S., Mauerhofer, A. M., Benedikt, F., & Hofbauer, H. (2019). The impact of gasification temperature on the process characteristics of sorption enhanced reforming of biomass. *Biomass Conversion and Biorefinery, 10*, 925–936.

Garcia-Vallejo, M. C., Rukh, M., Wang, S., Cai, R., Brody, L. G., Killmer, C., Lan, K., Yao, Y., Li, F., & Park, S. (2025). A new approach to improve the economic and environmental attractiveness of biomethane from biomass gasification with redox-activated CO_2 sorbents. *Chemical Engineering Journal*, Article 167510.

Gil, M. V., Fermoso, J., Pevida, C., Chen, D., & Rubiera, F. (2016). Production of fuel-cell grade H2 by sorption enhanced steam reforming of acetic acid as a model compound of biomass-derived bio-oil. *Applied Catalysis B: Environmental, 184*, 64–76.

Grasa, G. S., & Abanades, J. C. (2006). CO_2 capture capacity of CaO in long series of carbonation/calcination cycles. *Industrial & Engineering Chemistry Research, 45*, 8846–8851.

Gül, T., Remme, U., Menendez, J. M. B., Blanco, H., & Pizarro, A. (2025). *IEA Global hydrogen review 2025*. Paris https://www.iea.org/reports/global-hydrogen-review-2025 (Access. Apr. 7th, 2026).

Hanley, E. S., Deane, J. P., & Gallachóir, B. P.Ó. (2018). The role of hydrogen in low carbon energy futures–A review of existing perspectives. *Renewable and Sustainable Energy Reviews, 82*, 3027–3045.

Hosseini, S. E., & Wahid, M. A. (2016). Hydrogen production from renewable and sustainable energy resources: Promising green energy carrier for clean development. *Renewable and Sustainable Energy Reviews, 57*, 850–866.

House, K. Z., Harvey, C. F., Aziz, M. J., & Schrag, D. P. (2009). The energy penalty of post-combustion CO_2 capture & storage and its implications for retrofitting the U.S. installed base. *Energy & Environmental Science, 2*, 193.

Jiang, B., Dou, B., Wang, K., Zhang, C., Li, M., Chen, H., & Xu, Y. (2017). Sorption enhanced steam reforming of biodiesel by-product glycerol on Ni-CaO-MMT multifunctional catalysts. *Chemical Engineering Journal, 313*, 207–216.

Li, F., Cai, R., Rukh, M., Brody, L., & Yang, K. (2023). Multi-functional catalytic sorbents for hydrogen and hydrogen-enriched syngas production from carbon containing feedstock. *US patent, 63/503*, 508.

Li, H., Dang, C., Yang, G., Cao, Y., Wang, H., Peng, F., & Yu, H. (2021). Bi-functional particles for integrated thermo-chemical processes: Catalysis and beyond. *Particuology, 56*, 10–32.

Lundgren, J., Vreugdenhil, B., Ganjkhanlou, Y., & Baldwin, R. (2025). *IEA bioenergy T33 report*. Biomass Gasification for Hydrogen Production. https://www.ieabioenergy.com/blog/publications/biomass-gasification-for-hydrogen-production/ (Access. Apr.7th, 2026).

Mac Dowell, N., Sunny, N., Brandon, N., Herzog, H., Ku, A. Y., Maas, W., Ramirez, A., Reiner, D. M., Sant, G. N., & Shah, N. (2021). The hydrogen economy: A pragmatic path forward. *Joule, 5*, 2524–2529.

Masoudi Soltani, S., Lahiri, A., Bahzad, H., Clough, P., Gorbounov, M., & Yan, Y. (2021). Sorption-enhanced steam methane reforming for combined CO_2 capture and hydrogen production: A state-of-the-art review. *Carbon Capture Science & Technology, 1*, Article 100003.

Parthasarathy, P., & Narayanan, K. S. (2014). Hydrogen production from steam gasification of biomass: Influence of process parameters on hydrogen yield – A review. *Renewable Energy, 66*, 570–579.

Parvez, A. M., Hafner, S., Hornberger, M., Schmid, M., & Scheffknecht, G. (2021). Sorption enhanced gasification (SEG) of biomass for tailored syngas production with in-situ CO_2 capture: Current status, process scale-up experiences and outlook. *Renewable and Sustainable Energy Reviews, 141*, Article 110756.

Puig-Gamero, M., Argudo-Santamaria, J., Valverde, J. L., Sánchez, P., & Sanchez-Silva, L. (2018). Three integrated process simulation using aspen plus®: Pine gasification, syngas cleaning and methanol synthesis. *Energy Conversion and Management, 177*, 416–427.

Radfarnia, H. R., & Iliuta, M. C. (2014). Hydrogen production by sorption-enhanced steam methane reforming process using CaO-Zr/Ni bifunctional sorbent–catalyst. *Chemical Engineering and Processing: Process Intensification, 86*, 96–103.

Richardson, Y., Blin, J., & Julbe, A. (2012). A short overview on purification and conditioning of syngas produced by biomass gasification: Catalytic strategies, process intensification and new concepts. *Progress in Energy and Combustion Science, 38*, 765–781.

Rusten, H. K., Ochoa-Fernández, E., Lindborg, H., Chen, D., & Jakobsen, H. A. (2007). Hydrogen production by sorption-enhanced steam methane reforming using lithium oxides as CO_2-acceptor. *Industrial & Engineering Chemistry Research, 46*, 8729–8737.

Sazali, N. (2020). Emerging technologies by hydrogen: A review. *International Journal of Hydrogen Energy, 45*, 18753–18771.

Sikarwar, V. S., Pfeifer, C., Ronsse, F., Pohořelý, M., Meers, E., Kaviti, A. K., & Jeremiáš, M. (2022). Progress in in-situ CO_2-sorption for enhanced hydrogen production. *Progress in Energy and Combustion Science, 91*, Article 101008.

Sikarwar, V. S., Zhao, M., Clough, P., Yao, J., Zhong, X., Memon, M. Z., Shah, N., Anthony, E. J., & Fennell, P. S. (2016). An overview of advances in biomass gasification. *Energy & Environmental Science, 9*, 2939–2977.

Tezer, Ö., Karabağ, N., Öngen, A., Çolpan, C.Ö., & Ayol, A. (2022). Biomass gasification for sustainable energy production: A review. *International Journal of Hydrogen Energy, 47*, 15419–15433.

U.S. Department of Energy. (2023). *DOE national clean hydrogen strategy and roadmap*. https://www.hydrogen.energy.gov/library/roadmaps-vision/clean-hydrogen-strategy-roadmap (Access May. 7th, 2026).

Virginie, M., Adánez, J., Courson, C., de Diego, L. F., García-Labiano, F., Niznansky, D., Kiennemann, A., Gayán, P., & Abad, A. (2012). Effect of Fe–olivine on the tar content during biomass gasification in a dual fluidized bed. *Applied Catalysis B: Environmental, 121–122*, 214–222.

Wang, Y., Memon, M. Z., Seelro, M. A., Fu, W., Gao, Y., Dong, Y., & Ji, G. (2021). A review of CO2 sorbents for promoting hydrogen production in the sorption-enhanced steam reforming process. *International Journal of Hydrogen Energy, 46*, 23358–23379.

Wang, L., Zhou, T., Hou, B., Yang, H., Hu, N., & Zhang, M. (2025). A comprehensive review of biomass gasification characteristics in fluidized bed reactors: Progress, challenges, and future directions. *Fluid, 10*, 147.

Wu, G., Zhang, C., Li, S., Huang, Z., Yan, S., Wang, S., Ma, X., & Gong, J. (2012). Sorption enhanced steam reforming of ethanol on Ni–CaO–Al_2O_3 multifunctional catalysts derived from hydrotalcite-like compounds. *Energy & Environmental Science, 5*, 8942.

Yan, Y., Manovic, V., Anthony, E. J., & Clough, P. T. (2020). Techno-economic analysis of low-carbon hydrogen production by sorption enhanced steam methane reforming (SE-SMR) processes. *Energy Conversion and Management, 226*, Article 113530.

Yang, X., Kan, T., Kheradmand, A., Xu, H., Strezov, V., Yu, A., & Jiang, Y. (2021). Tunable syngas production from two-stage sorption-enhanced steam gasification of sewage sludge. *Chemical Engineering Journal, 404*.

Yue, M., Lambert, H., Pahon, E., Roche, R., Jemei, S., & Hissel, D. (2021). Hydrogen energy systems: A critical review of technologies, applications, trends and challenges. *Renewable and Sustainable Energy Reviews, 146*, Article 111180.

Zapantis, A. (2021). *Circular carbon economy series: Blue hydrogen*. https://www.globalccsinstitute.com/wp-content/uploads/2021/04/Circular-Carbon-Economy-series-Blue-Hydrogen.pdf (Access. Apr. 7th, 2026).

Zhao, X., Zhou, H., Sikarwar, V. S., Zhao, M., Park, A.-H. A., Fennell, P. S., Shen, L., & Fan, L.-S. (2017). Biomass-based chemical looping technologies: The good, the bad and the future. *Energy & Environmental Science, 10*, 1885–1910.